# On the representation of electron multiple elastic-scattering distributions for Monte Carlo calculations

Iwan Kawrakow [*], Alex F. Bielajew [1]

*Institute for National Measurement Standards, Ionizing Radiation Standards, National Research Council of Canada, Ottawa, Canada K1A 0R6*

## Abstract

A new representation of elastic electron–nucleus (Coulomb) multiple-scattering distributions is developed. Using the screened Rutherford cross section with the Molière screening parameter as an example, a simple analytic angular transformation of the Goudsmit–Saunderson multiple-scattering distribution accounts for most of the structure of the angular distribution leaving a residual 3-parameter (path-length, transformed angle and screening parameter) function that is reasonably slowly varying and suitable for rapid, accurate interpolation in a computer-intensive algorithm. The residual function is calculated numerically for a wide range of Molière screening parameters and path-lengths suitable for use in a general-purpose condensed-history Monte Carlo code. Additionally, techniques are developed that allow the distributions to be scaled to account for energy loss. This new representation allows "on-the-fly" sampling of Goudsmit–Saunderson angular distributions in a screened Rutherford approximation suitable for Class II condensed-history Monte Carlo codes. Published by Elsevier Science B.V.

## 1. Introduction

In this article we consider the representation of multiple elastic-scattering distributions as employed by condensed-history Monte Carlo methods. The foundations of the condensed-history

Monte Carlo method were first discussed in detail by Berger [1]. The condensed-history technique treats the cumulative effect of many elastic and inelastic collisions in one step by sampling from cumulative deflection or energy-loss distributions, thus saving computation time. The improbable interactions that cause a sudden change in electron energy, typically Møller and bremsstrahlung interactions, can be considered to be discrete events and Berger defined two classes of electron condensed-history algorithms by the way with which these large energy-loss interactions are treated.

---

[*] Corresponding author. Tel.: 613 993 2197; fax: 613 952 9865; e-mail: iwan@irs.phy.nrc.ca.

[1] Present address: Department of Nuclear Engineering and Radiological Sciences, The University of Michigan, Cooley Building, 2355 Bonisteel Boulevard, Ann Arbor, Michigan, USA.

The essential difference insofar as this work is concerned is that Class I algorithms transport electrons along a predetermined energy-loss grid, and the multiple-scattering probability distributions for these grid points may be computed before the simulation of electron transport, thereby saving computer time and improving run-time efficiency. The multiple-scattering probability distributions may be calculated using the Goudsmit–Saunderson's formalism [2,3] using the latest elastic cross sections. This approach yields "exact" multiple-scattering distributions according to the single-scattering law, assuming that the numerical accuracy can be controlled. Offsetting this positive attribute are a lack of correlation between the primary and secondary particles, the necessity to interpolate distributions when the electron energy does not conform to the grid, and approximate treatment of the crossing of interfaces. Class II algorithms are in principle more accurate since all distributions are sampled "on-the-fly" as the distance between interaction points is treated as a stochastic quantity, and the angular distributions for any path-length may be required. Calculated differences between Class I and Class II algorithms are not seen except for certain specialized applications and further discussion is not germane to the present discussion. A more complete discussion of Class I vs. Class II is given elsewhere [4].

Since Class II algorithms require the sampling of angular distributions for any electron path-length, this technique has favored the employment of multiple-scattering theory formulated in the small-angle approximation with a specialization to the screened Rutherford cross section, as these functional forms may be sampled with reasonable speed during iterative computations. The usual choice of multiple-scattering formalism is that of Molière's [5], which can express all kinematic parameters (energy, atomic number, angle, distance) in terms of just two scaled parameters, providing a very compact and efficient form. [2]

However, it is known that Molière's theory has constraints for both large and small path-lengths [7]. Although the Molière formalism is adequate for many applications, the small-path-length constraint is a severe limitation for some interface studies, and the large-path-length constraint leads to slow execution of Monte Carlo codes, particularly for high-$Z$ applications. The breakdown of Molière's formalism has been studied [8]. Bielajew has reformulated small-angle multiple scattering theory in such a way as to eliminate the small-path-length difficulties [6,9] and some of those techniques are incorporated herein but within the any-angle formalism of Goudsmit and Saunderson [2,3].

In this report we discuss a new multiple-scattering formalism that allows Class II algorithms to sample angular distributions using the any-angle formalism of Goudsmit and Saunderson [2,3]. We specialize to the screened Rutherford cross section [10] using the Molière screening angle [11]. The choice of cross section is not an essential approximation but it serves as a concrete example with much inherent application. The inclusion of spin and relativistic corrections via Mott cross sections [12,13] or more recent compilations [10,14] is left for later work. Additionally, we introduce energy loss in the continuous slowing down approximation (CSDA) in such a way as to retain compatibility with Class II condensed-history algorithms and allow large condensed-history steps involving appreciable energy loss – up to 25% with little loss of accuracy. For preparation, we start with a general discussion of multiple-scattering theories, showing the connection between the various formulations.

## 2. Multiple-scattering theories

### 2.1. The small-angle approximation

Bothe [15] and Wentzel [16] have described a theory of small-angle multiple elastic scattering which provides the probability for scattering into an angular interval $d\theta$ at an angle $\theta$ after a total path-length corresponding to $\lambda$ mean-free-paths:

---

[2] It can be shown that this characteristic is general for small-angle multiple-scattering distributions using screened Rutherford cross sections. Molière's theory is just one expression of that property [6].

$$F_{SA}(\theta, \lambda)\theta \, d\theta = d\theta \, \theta \int\limits_0^\infty d\eta \, \eta \, J_0(\eta\theta)$$

$$\times \exp\left(-\lambda \int\limits_0^\infty d\chi \, \chi \, \tilde{\sigma}(\chi)[1 - J_0(\eta\chi)]\right), \qquad (1)$$

where $J_0$ is the Bessel function of zeroth order and $\tilde{\sigma}(\chi)$ the single-scattering law normalized to unity, [3]

$$\tilde{\sigma}(\chi) = \frac{\sigma(\chi)}{\int\limits_0^\pi d\chi \, \sin \chi \sigma(\chi)}. \qquad (2)$$

This approximate expression has been used by Molière to derive an analytic expansion of Eq. (1) with respect to a parameter $B$ depending on $\lambda$ [5]. Because of its simple analytic form and the little amount of pre-calculated data required, Molière's theory has found widespread use in electron and proton transport models. To overcome the breakdown of Molière's theory at small pathlengths, Bielajew developed an exact numerical solution of Eq. (1) for use in Monte Carlo simulations [6,9]. Although this theory represents an improvement of the modeling of multiple electron scattering, it remains a small-angle approximation with decreasing accuracy for increasing electron step-sizes and/or decreasing energies.

## 2.2. The any-angle formalism

Goudsmit and Saunderson [2,3] presented a formal solution of the multiple-scattering problem in the form of an expansion in Legendre polynomials $P_l(\cos \theta)$, which is valid for any-angle scattering

$$F_{GS}(\cos \theta) = \sum_{l=0}^\infty \left(l + \frac{1}{2}\right) P_l(\cos \theta) \exp(-\lambda Q_l), \qquad (3)$$

where $Q_l$ denotes the moments of the single-scattering distribution,

$$Q_l = \int\limits_{-1}^1 d(\cos \chi)\tilde{\sigma}(\cos \chi)[1 - P_l(\cos \chi)]. \qquad (4)$$

Bethe [7] and Winterbon [17] have discussed some of the approximations required to obtain the small-angle expression, Eq. (1), from the Goudsmit–Saunderson (GS) series. Bethe has proposed a correction factor $\sqrt{\sin \theta/\theta}$ to improve the small-angle multiple-scattering approximation at large angles, while Winterbon discusses higher-order corrections.

## 2.3. The small momentum transfer approximation

Kawrakow [18] performed a Wentzel-type analysis using the momentum transfer instead of the scattering angle as the angular variable. The connection between the momentum transfer $q$ and the scattering angle $\theta$ is given by,

$$q^2 = 2p^2(1 - \cos \theta), \qquad (5)$$

$p$ being the electron's momentum. The resulting multiple-scattering distribution in the small-angle approximation is:

$$F_{SAq}(q, \lambda)q \, dq = dq \, q \int\limits_0^\infty db \, b \, J_0(bq)$$

$$\times \exp\left(-\lambda \int\limits_0^\infty dq' \, q' \, \tilde{\sigma}(q')[1 - J_0(q'b)]\right). \qquad (6)$$

For small scattering angles $q \approx p\theta$ and the above expression is equivalent to Eq. (1). It was concluded in Ref. [18] that Eq. (6) has advantages compared to Eq. (1) due to the fact that the any-angle form of the single-scattering cross section can be used to evaluate the integral in the exponential. In this paper we will show that Eq. (6) yields an exact description of the multiple-scattering distribution at all angles when the small-angle approximation is justified (see the condition (7) below).

Two approximations are required to obtain Eq. (6) from the GS-series: (a) the replacement of the summation by an integral and (b) the approximation of the Legendre polynomials by the Bessel

---

[3] When $\sigma(\chi)$ is used in its small-angle approximation and the small-angle integral is convergent, the form $\tilde{\sigma}(\chi) = \sigma(\chi)/\int_0^\infty d\chi \, \chi\sigma(\chi)$ may be used.

function of zeroth order $J_0$. Concerning (a), Euler's summation formula [19] may be used. Higher-order corrections will be small when a large number of terms is required to obtain convergence of the GS-series. Convergence of the GS-series is obtained for $l > (\lambda Q_1)^{-1/2}$ (see Ref. [20] and the discussion below) where $Q_1$ is defined in Eq. (4). That is, the first condition for the applicability of the small-angle approximation is

$$\lambda Q_1 = \lambda \langle 1 - \cos \chi \rangle \ll 1. \tag{7}$$

Here, $\langle \; \rangle$ means averaging with respect to the single-scattering law. The above condition will be satisfied when both the average angle in a single-scattering event and the average multiple-scattering angle are small.

The approximation (b) affects the evaluation of the GS-moments $Q_l$ in the exponent of Eq. (3) and the summation itself. To investigate the errors introduced by (b) we first note that Eq. (6) can be transformed to

$$F_{\mathrm{SA}q}(\cos \theta, \lambda) = \int\limits_0^\infty \mathrm{d}z \, z \, J_0\Big(z\sqrt{2(1 - \cos \theta)}\Big)$$
$$\times \exp\big(-\lambda Q_{\mathrm{SA}q}(z)\big), \tag{8}$$

where we have defined

$$Q_{\mathrm{SA}q}(z) = \int \mathrm{d}\chi \, \sin \chi \, \tilde{\sigma}(\cos \chi)$$
$$\times \Big[1 - J_0\Big(z\sqrt{2(1 - \cos \chi)}\Big)\Big]. \tag{9}$$

We can then compare the power series expansion of the zeroth order Bessel function to the expansion of the Legendre polynomials:

$$J_0\Big(z\sqrt{2(1 - \cos \theta)}\Big) \approx 1 - \frac{l(l+1)}{4}\theta^2$$
$$+ \left(\frac{l(l+1)}{48} + \frac{l^2(l+1)^2}{64}\right)\theta^4$$
$$- \left(\frac{l(l+1)}{1440} + \frac{l^2(l+1)^2}{384} + \frac{l^3(l+1)^3}{2304}\right)\theta^6 \pm \cdots, \tag{10}$$

$$P_l(\cos \theta) \approx 1 - \frac{l(l+1)}{4}\theta^2$$
$$+ \left(\frac{l(l+1)}{48} + \frac{(l-1)l(l+1)(l+2)}{64}\right)\theta^4$$
$$- \left(\frac{l(l+1)}{1440} + \frac{(l-1)l(l+1)(l+2)}{384}\right.$$
$$+ \left.\frac{(l-2)(l-1)l(l+1)(l+2)(l+3)}{2304}\right)\theta^6 \pm \cdots \tag{11}$$

In the first equation we have made use of $z^2 = l(l+1)$. With this formulas we have

$$Q_l \approx \frac{l(l+1)}{4}\langle \chi^2 \rangle$$
$$- \left(\frac{l(l+1)}{48} + \frac{(l-1)l(l+1)(l+2)}{64}\right)\langle \chi^4 \rangle \pm \cdots,$$
$$Q_{\mathrm{SA}q} \approx \frac{l(l+1)}{4}\langle \chi^2 \rangle$$
$$- \left(\frac{l(l+1)}{48} + \frac{l^2(l+1)^2}{64}\right)\langle \chi^4 \rangle \pm \cdots \tag{12}$$

Here, $\langle \; \rangle$ means again averaging over the single-scattering cross section. For small-angle scattering, $\langle \chi^4 \rangle \ll \langle \chi^2 \rangle$ and therefore the terms proportional to $\langle \chi^4 \rangle$ are only small corrections for small $l$. On the other hand, the difference between $l(l+1)$ and $(l-1)(l+2)$ is negligible for large $l$ (this is of course true also for the higher-order terms, not shown in Eq. (12) for the sake of brevity). We can therefore conclude that $Q_{\mathrm{SA}q}$ represents a sufficiently accurate approximation to $Q_l$ for any $l$ when the small-angle approximation is justified (see also Eq. (18) and the subsequent discussion below).

Concerning the summation, it is important to realize that terms with large $l$ are more important when condition (7) is satisfied. To see this, we write Eq. (3) in the form $F_{\mathrm{GS}}(\cos \theta) = \sum_{l=0}^{\infty} w_l P_l(\cos \theta)$ with

$$w_l = \left(l + \frac{1}{2}\right)\exp(-\lambda Q_l)$$
$$\approx \left(l + \frac{1}{2}\right)\exp\left[-\frac{\lambda\langle \chi^2 \rangle}{4}\left(l + \frac{1}{2}\right)^2\right]$$
$$\times \exp(-\lambda\langle \chi^2 \rangle/16). \tag{13}$$

Here, we have made use of Eq. (12). It is obvious that Legendre polynomials around $l_{max}$,

$$l_{max} = \sqrt{\frac{2}{\lambda \langle \chi^2 \rangle}} - \frac{1}{2} \approx \sqrt{\frac{1}{\lambda Q_1}}, \qquad (14)$$

will give the most important contribution to the summation since $w_l$ has a maximum. [4] If condition (7) is satisfied, $l_{max}$ is large and therefore the most important contributions to the GS-series will come from terms with large $l$ where we can neglect the difference between $l(l+1)$ and $(l-1)(l+2)$, $(l-2)(l+3)$, etc. In this case, the power series expansion of $J_0$ almost exactly matches the power series expansion of the Legendre polynomials (this holds also for higher-order terms not shown in Eqs. (10) and (11)). Therefore, the replacement of the Legendre polynomials by the Bessel function will be sufficiently accurate and we expect good agreement between the exact multiple-scattering distribution and the small-angle approximation when the condition expressed by Eq. (7) is satisfied.

To be more concrete, let us consider the case where the screened Rutherford cross section is used to describe single scattering, i.e.

$$\tilde{\sigma}(\cos \chi) = \frac{2\eta(1+\eta)}{(1 - \cos \chi + 2\eta)^2}, \qquad (15)$$

where $\eta$ is the screening parameter (we use the notation of Berger and Wang [10]). In this case the GS-moments $Q_l$ are given by

$$Q_l = 1 - \frac{1+\eta}{\eta^{l+1}} \frac{\Gamma(l+1)\Gamma(l+2)}{\Gamma(2l+2)}$$
$$\times {}_2F_1\left(l+1, l+2, 2l+2, -\frac{1}{\eta}\right), \qquad (16)$$

where ${}_2F_1$ is the hypergeometric function. In comparison, the small-angle moments $Q_{SAq}$ read

$$Q_{SAq}(y) = 1 - yK_1(y), \quad y = 2\sqrt{l(l+1)\eta}, \qquad (17)$$

where $K_1$ a modified Bessel function. To investigate the differences between both expressions, we

have expanded the ratio $Q_l/Q_{SAq}$ in a power series of the screening parameter $\eta$. The result is

$$Q_l = 1 - yK_1(y)\left[1 + 2\eta l(l+1)\right.$$
$$\times \left.\left(\Psi(l) - \frac{1}{2}\ln[l(l+1)]\right) \pm \cdots\right], \qquad (18)$$

where $\Psi(l)$ is the logarithmic derivative of the gamma function,

$$\Psi(l) = \frac{d \ln \Gamma(l+1)}{dl} = -\gamma + 1 + \frac{1}{2} + \cdots + \frac{1}{l}, \quad (19)$$

where $\gamma = 0.5772\ldots$ is Euler's constant. The term in the square brackets proportional to $\eta$ is a monotonically increasing function of $l$ which approaches $1/6$ for $l \to \infty$. Because for most physically relevant situations $\eta \ll 1$, the first order correction to the small-angle approximation is always small. The ratio $(Q_{SAq} - Q_l)/Q_{SAq}$ which expresses the relative error has a maximum for $l = 1$ given by

$$\frac{Q_{SAq}(l=1) - Q_1}{Q_{SAq}(l=1)}$$
$$= \frac{4\eta(1 - \gamma - \ln(2)/2)\sqrt{8\eta}K_1(\sqrt{8\eta})}{1 - \sqrt{8\eta}K_1(\sqrt{8\eta})} \pm \cdots$$
$$\approx \frac{2 - 2\gamma - \ln(2)}{1 - 2\gamma - \ln(2\eta)}. \qquad (20)$$

For $\eta$ as large as 0.01 (e.g. 2 keV electrons in water) the error is of the order of 4% being much smaller at higher energies.

Finally, we have calculated the multiple-scattering distributions $F_{GS}$ according to Eq. (3) and $F_{SAq}$ from Eq. (8) respectively, using the screened Rutherford cross section and different values of $\xi = \lambda Q_1$. The ratio $F_{GS}/F_{SAq}$ is shown in Fig. 1(a) for $\xi = 0.001$ and in Fig. 1(b) for $\xi = 0.2$. The latter value of $\xi$ corresponds to a typical condensed-history path-length for the simulation of electron transport in low $Z$ materials (e.g. graphite) at low energies (a few keV to a few hundred keV). The former has been chosen in order to demonstrate that $F_{GS}$ in fact converges to $F_{SAq}$ when the small-angle approximation is justified ($\xi \ll 1$). To show the strong improvement when using the momentum transfer as the angular variable, also

---

[4] If we take into account terms proportional to $\langle \chi^4 \rangle$ and higher in the evaluation of $Q_l$, $l_{max}$ is shifted towards even larger values of $l$.

## Angular distribution ratios
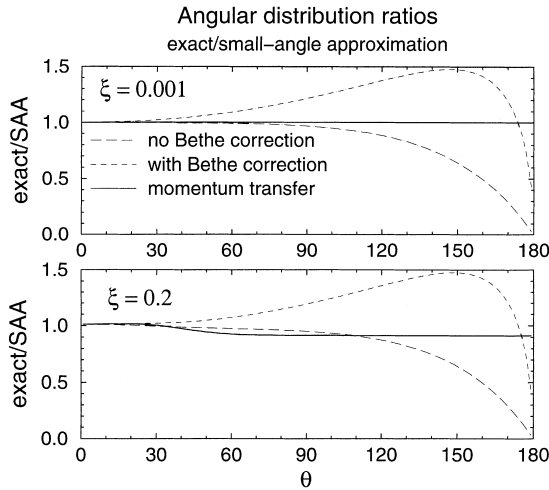### exact/small–angle approximation



Fig. 1. The ratio of the exact MS-distribution to the MS-distribution in a small-angle approximation using the momentum transfer as the angular variable, $F_{GS}/F_{SAq}$, calculated from Eqs. (3) and (8) for $\xi = 0.001$ (top figure) and $\xi = 0.2$ (bottom figure). For comparison, the same ratio calculated with the scattering angle as the angular variable with (short-dash line) and without (long-dash line) Bethe correction is shown.

the small-angle results from the scattering angle formulation with and without Bethe correction are shown in these figures. For $\xi = 0.001$ the maximum deviation between $F_{GS}$ and $F_{SAq}$ is 0.2%. It is very interesting to observe that the deviations between $F_{GS}$ and $F_{SAq}$ grow to approximately 10% when changing the screening parameter by 3 order of magnitude! This fact will allow us to construct a method for sampling the multiple-scattering angle from the exact distribution for arbitrary path-lengths with a relatively small amount of pre-calculated data. The procedure is described in the next section.

## 3. Any-angle hybrid multiple-scattering theory

In Refs. [6,9] Bielajew developed a new small-angle approach to multiple scattering. In this paper we will extend the formalism of Refs. [6,9] to allow for the sampling of the multiple-scattering angle from the exact distribution using the any-angle form of the screened Rutherford cross section.

### 3.1. General formulae

There are two steps necessary to obtain the $q^{(2+)}$-surface used in Ref. [9] to describe the multiple-scattering distribution:

(i) Subtract the no-scattering and single-scattering contributions from the multiple-scattering distribution, i.e.

$$\begin{aligned} F_{GS}(\cos\theta) = {}& e^{-\lambda}\delta(1 - \cos\theta) \\ & + \lambda e^{-\lambda}\tilde{\sigma}(\cos\theta) \\ & + \left(1 - \lambda - \lambda e^{-\lambda}\right)F_{GS}^{(2+)}(\cos\theta). \end{aligned} \quad (21)$$

The distribution for at least two collisions, $F_{GS}^{(2+)}$, is

$$F_{GS}^{(2+)}(\cos\theta) = \sum_{l=0}^{\infty}\left(l + \frac{1}{2}\right)P_l(\cos\theta)j_l^{(2+)} \quad (22)$$

with the short hand notation

$$\begin{aligned} &j_l^{(2+)} \\ &= \frac{\exp(-\lambda Q_l) - [1 + \lambda(1 - Q_l)]\exp(-\lambda)}{1 - \exp(-\lambda) - \lambda\exp(-\lambda)}. \end{aligned} \quad (23)$$

The explicit extraction of the single-scattering term suggests the adjective "hybrid" since in the regime of small path-lengths the multiple-scattering distribution is dominated explicitly by the single-scattering distribution. This may be exploited by geometry-adaptive electron-transport algorithms such as PRESTA [21,22] or Seltzer's TLC (Transverse and Longitudinal Correction) [23] to effect the crossing of material (or scoring) boundaries. As a boundary is approached the condensed-history algorithm "evaporates" into a single-scattering algorithm. The combination of single-scattering and multiple-scattering algorithms into a single formalism is therefore a hybrid method that can exploit both the computational efficiency of multiple-scattering theories with the accuracy of a single-scattering approach.

(ii) A variable change which makes the 2+ scattering distribution "flat" and easy for numerical evaluation.

Concerning (ii), in Refs. [6,9] the variable transformation

$$u = 1 - \frac{\chi_a^2 w^2}{\theta^2 + \chi_a^2 w^2} \quad (24)$$

was employed. This was motivated by the use of the screened Rutherford cross section to describe single scattering and by the fact that the multiple-scattering distribution at large angles is determined mainly by the single-scattering law. We have namely

$$\mathrm{d}u = \frac{2w^2\chi_a^2\theta\,\mathrm{d}\theta}{(\theta^2 + w^2\chi_a^2)^2}, \tag{25}$$

which looks like a single-scattering cross section with a screening angle increased by the "spreading" parameter $w$. The formalism of Refs. [6,9] can be generalized to arbitrary variable transformations

$$u = f(a_1, \ldots, a_n; \mu), \tag{26}$$

where $a_1, \ldots, a_n$ are some parameters characterizing the transformation and $\mu$ is a short hand notation for $\cos\theta$. We will denote the 2+ distribution in the variable $u$ by $q^{(2+)}$, i.e.

$$q^{(2+)}(u)\,\mathrm{d}u = F_{\mathrm{GS}}^{(2+)}(\mu)\,\mathrm{d}\mu \tag{27}$$

or

$$q^{(2+)}(u) = F_{\mathrm{GS}}^{(2+)}(\mu)\left(\frac{\partial f(a_1, \ldots, a_n; \mu)}{\partial\mu}\right)^{-1}. \tag{28}$$

The parameters $a_1, \ldots, a_n$ can be fixed from the requirement that $q^{(2+)}(u)$ is as close to unity as possible, i.e. by minimizing the function $r^2(a_1, \ldots, a_n)$,

$$r^2(a_1, \ldots, a_n) = \int \mathrm{d}u(q^{(2+)}(u) - 1)^2. \tag{29}$$

This leads to the following set of $n$ equations

$$\int\limits_{-1}^{1}\mathrm{d}\mu\left[F_{\mathrm{GS}}^{(2+)}(\mu)\left(\frac{\partial f(a_1, \ldots, a_n; \mu)}{\partial\mu}\right)^{-1}\right]^2$$
$$\times\frac{\partial^2 f(a_1, \ldots, a_n; \mu)}{\partial\mu\,\partial a_i} = 0, \quad i = 1, \ldots, n. \tag{30}$$

The above formalism can be used with any single-scattering law. However, to guess the appropriate variable transformation, it is necessary to know the single-scattering distribution analytically. This may make it difficult to combine the results of this paper with single-scattering cross sections from partial-wave analysis [10]. On the

other hand, the use of the condensed-history technique and multiple-scattering theories is meaningful only for problems that involve a large number of collisions of electrons with surrounding matter. In this case, the precise shape of the single-scattering law becomes less and less important and the electron-transport problem under consideration can be well described in terms of the first few moments of the single-scattering distribution. For instance, the average transition in the initial direction of motion $\langle s \rangle$ is determined completely by the first moment $\lambda Q_1$, the average lateral displacement $\langle r^2 \rangle$ as well as $\langle s \cos\theta \rangle$, $\langle s^2 \rangle$, $\langle r \sin\theta \rangle$ by the first and second moments of the single-scattering law [20]. It seems therefore justified to use a simplified single-scattering cross section which describes the first few moments correctly.

### 3.2. Multiple scattering from the screened Rutherford cross section

In this section we will apply the formalism developed above to the special case where single scattering is described by the screened Rutherford cross section. In this case we can use the variable transformation

$$f(a; \mu) = (1 + a)\left(1 - \frac{2a}{1 - \mu + 2a}\right), \quad a = w^2\eta \tag{31}$$

which is the any-angle form analogous to Eq. (24). We have then for the derivatives

$$\frac{\partial f(a; \mu)}{\partial\mu} = -\frac{2a(1 + a)}{(1 - \mu + 2a)^2},$$
$$\frac{\partial^2 f(a; \mu)}{\partial\mu\,\partial a} = -2\frac{1 - \mu(1 + 2a)}{(1 - \mu + 2a)^3}. \tag{32}$$

Inserting the above equations into Eq. (30) and solving with respect to $a$ we obtain

$$a = \kappa + \sqrt{\kappa^2 + \kappa} \tag{33}$$

with the short hand notation

$$\kappa = \frac{\langle 0 \rangle - 2\langle 1 \rangle + \langle 2 \rangle}{4\langle 1 \rangle} \tag{34}$$

and

$$\langle n \rangle = \sum_{l=0}^{\infty} \left( l + \frac{1}{2} \right) j_l^{(2+)}$$

$$\times \sum_{m=0}^{\infty} \left( m + \frac{1}{2} \right) j_m^{(2+)} \int_{-1}^{1} \mathrm{d}\mu \, \mu^n P_l(\mu) P_m(\mu), \quad (35)$$

where $j_l^{(2+)}$ was defined in Eq. (23). Using the properties of the Legendre polynomials we can simplify the expression for the $\langle n \rangle$'s necessary to calculate $\kappa$:

$$\langle 0 \rangle = \sum_{l=0}^{\infty} \left( l + \frac{1}{2} \right) [j_l^{(2+)}]^2,$$

$$\langle 1 \rangle = \sum_{l=0}^{\infty} (l+1) j_l^{(2+)} j_{l+1}^{(2+)}, \quad (36)$$

$$\langle 2 \rangle = \sum_{l=0}^{\infty} \frac{(l+1/2)(2l^2+2l-1)}{(2l+3)(2l-1)} [j_l^{(2+)}]^2$$

$$+ \sum_{l=0}^{\infty} \frac{(l+1)(l+2)}{2l+3} j_l^{(2+)} j_{l+2}^{(2+)}.$$

Whereas in the small-angle formulation the spreading parameter is only a function of $\lambda$, now $w^2 = a/\eta$ depends on $\lambda$ and $\eta$. However, due to arguments similar to those given in Section 2.3 when discussing the multiple-scattering distribution, for $\xi = \lambda Q_1 \to 0$, $w^2$ converges to the value derived from the small-angle approximation, $w_{SA}$, and changes slowly as $\xi$ is changed (increased). This is demonstrated in Fig. 2 where the ratio $w/w_{SA}$ for various values of $\xi$ is depicted as a function of $\lambda$. The upper limit $\lambda = 10^5$ chosen to calculate $\omega$ should be sufficient for any practical application. The lower limit $\lambda = 1$ was determined by efficiency considerations: for path-lengths smaller than 2-3 elastic mean-free-paths, a detailed (event-by-event) simulation of elastic scattering becomes computationally more efficient than a condensed-history simulation.

For completeness we give also the explicit formula for $q^{(2+)}$ resulting from the transformation Eq. (31):

$$q^{(2+)}(u, \lambda, a) = \frac{2a(1+a)}{(1+a-u)^2} \sum_{l=0}^{\infty} \left( l + \frac{1}{2} \right)$$

$$\times P_l \left[ \frac{1+a-(1+2a)u}{1+a-u} \right] j_l^{(2+)}(\lambda, a). \quad (37)$$
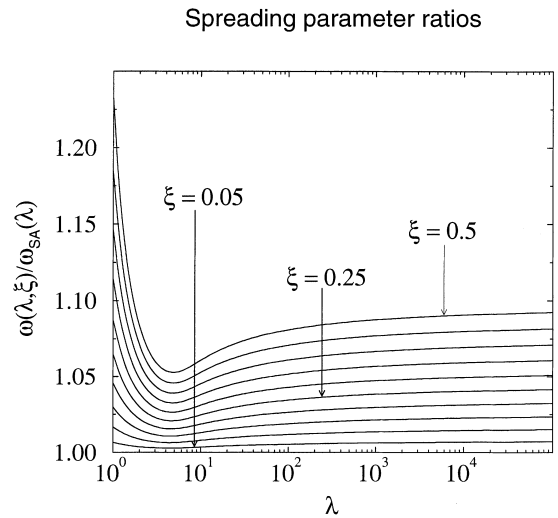


Fig. 2. The ratio of the spreading parameter $w(\lambda, \xi)$ calculated according to Eqs. (33)–(35), to the spreading parameter $w_{SA}(\lambda)$ resulting from a small-angle approximation.

In Fig. 3, $q^{(2+)}$-curves for three different $\lambda$'s and various values of the screening parameter are shown. The curves labeled as "small-angle limit" (thick lines) were calculated for a screening parameter $\eta = 2.618 \times 10^{-5}$ ($\lambda = 10$), $1.715 \times 10^{-7}$ ($\lambda = 10^3$) and $1.284 \times 10^{-9}$ ($\lambda = 10^5$) giving $\xi = \lambda Q_1 = 5 \times 10^{-4}$ in all cases. For even smaller val-
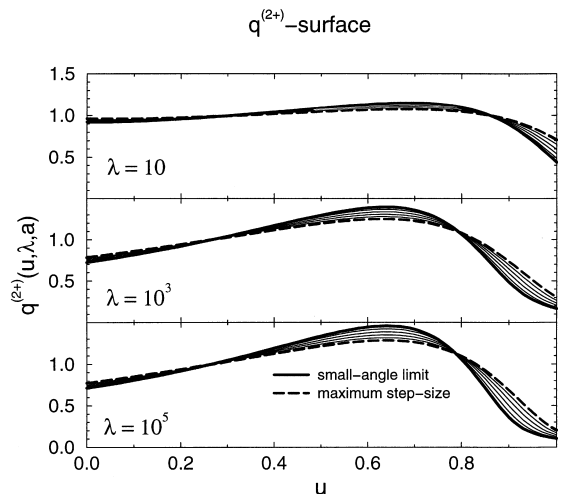


Fig. 3. $q^{(2+)}$ surfaces for $\lambda = 10$, $10^3$ and $10^5$. For explanation of the labels "small-angle limit" and "maximum step-size", see text.

ues of $\eta$ (or $\xi$) the calculated $q^{(2+)}$ did not change within the numerical precision (0.1% for $u \to 1$ when using double precision variables). The curves labeled as "maximum step-size" represent the situation where $\xi = 0.5$ corresponding to an average multiple-scattering angle of about one radian. This is considered to be the maximum acceptable step-size because for even larger average multiple scattering angles the application of the condensed-history technique becomes more and more questionable. Curves depicted with thin lines correspond to intermediate values of $\xi$ uniformly distributed between 0 and 0.5. This figure confirms the conclusion of Section 2.3 that the variation of the multiple-scattering distribution with the screening parameter is rather slow once the variable transformation is effected.

### 3.3. Numerical implementation

In this section we will discuss some aspects of the numerical calculations necessary to obtain the spreading parameter $\omega$ and the $q^{(2+)}$-surface, as well as the implementation of the model for multiple-scattering sampling in Monte Carlo simulations.

We start with the calculation of the GS-moments $Q_l$. For the screened Rutherford cross section the iterative procedure derived by Spencer [24] could be used:

$$Q_0 = 0,$$

$$Q_1 = 2\eta \left[ \ln\left(1 + \frac{1}{\eta}\right)(1 + \eta) - 1 \right],$$

$$(l-1)Q_l = (2l-1)(1+2\eta)Q_{l-1} - lQ_{l-2}$$
$$- 2\eta(2l-1), \quad l \geqslant 2. \tag{38}$$

However, due to round-off errors, this method breaks down for $l > \sim 1000$ even when using double precision variables. A similar effect occurred when we tried to evaluate Eq. (16) with the Mathematica code system [25]. For small number of elastic collisions and/or very small $\eta$, much more than 1000 terms are necessary to obtain convergence of the GS-series. We decided therefore to use Eq. (18) to calculate the GS-moments. This expression is accurate to $O(\eta^2)$ and because $\eta$ is a small quantity for most relevant situations, this represents a very

good approximation. We compared the multiple-scattering distribution calculated with Spencer's iterative procedure to the distribution obtained using Eq. (18) to calculate $Q_l$ in various cases where less than 1000 terms were necessary for the convergence of the series, and found an agreement to better than 0.3% for all situations studied.

In Refs. [6,9] the $q^{(2+)}$-surface was calculated only for $\lambda \leqslant 3050$. This limitation was caused by numerical instabilities for larger $\lambda$-values. In the present work, due to the use of the exact expressions rather than small-angle approximations, integrations are replaced by summations which can be performed more easily and reliably. We were able to calculate the spreading parameter $\omega$ and the $q^{(2+)}$-surface for arbitrary $\lambda$ without observing any numerical problems and used $\lambda = 10^5$ as our upper limit for practical considerations.

For the multiple-scattering angle sampling on-the-fly, a fast calculation of the $q^{(2+)}$-surface for arbitrary $\lambda$ and $\eta$ values is required. This can be done by a linear interpolation between pre-calculated $q^{(2+)}$-curves on a given ($\lambda$–$\eta$) grid. The density of this grid depends on the required accuracy. For instance, to obtain an accuracy of 0.2% or better of the interpolated $q^{(2+)}$-curves, 16 subdivisions per decade in $\lambda$-direction are necessary. For every $\lambda$ value, 11 different screening parameters are used to calculate $q^{(2+)}$ at 101 $u$-points. That means, to score the pre-calculated data in the range $1 \leqslant \lambda \leqslant 10^5$ approximately 360 kB of computer memory are necessary.

## 4. Energy loss

To take the energy loss of electrons during the step into consideration, we have to replace $\lambda Q_l$ in the exponent of Eq. (3) by

$$G_l = 2\pi N \int_0^t \mathrm{d}t' \int_{-1}^1 \mathrm{d}(\cos \chi)$$
$$\times \sigma(\cos \chi, t')[1 - P_l(\cos \chi)], \tag{39}$$

where $N$ is the number of atoms per unit volume and $t$ the path-length. The dependence of the single-scattering cross section $\sigma(\cos \chi, t')$ on the ener-

gy is expressed through the dependence on the path-length $t'$. Although, in principle, it is possible to use $G_l$ instead of $\lambda Q_l$ to calculate the $q^{(2+)}$-surface, this approach would not be efficient on a present-day computer due to the large increase of memory required to score the pre-calculated data. In fact, when we take energy loss into account, the dependence of the multiple-scattering distribution on the screening parameter $\eta$ alone is replaced by a dependence on the energy *and* the material in which the transport takes place. Therefore, one additional dimension will be needed to store the pre-calculated data. We will therefore approximate $G_l$ in such a way that the application of the method presented in the last section becomes possible.

We rewrite Eq. (39) as

$$
\begin{aligned}
G_l &= 2\pi N \int\limits_{E_f}^{E_i} \frac{\mathrm{d}E}{S(E)} \sigma_{\mathrm{tot}}(E) \\
&\quad \times \int\limits_{-1}^{1} \mathrm{d}(\cos\chi)\tilde{\sigma}(\cos\chi, E)[1 - P_l(\cos\chi)] \\
&= b_c \int\limits_{E_f}^{E_i} \frac{\mathrm{d}E}{S(E)\beta^2} Q_l(E).
\end{aligned}
\tag{40}
$$

Here, $E_i$ and $E_f$ are the initial and final kinetic energies of the electron, $S(E)$ the restricted collision stopping power, [5] $\sigma_{\mathrm{tot}}(E)$ the total elastic cross-section and $\tilde{\sigma}$ is again normalized to unity. To arrive at the second equation, we have made use of the fact that $\sigma_{\mathrm{tot}}$ is proportional to $1/\beta^2$ where $\beta$ is the electron's velocity in units of the velocity of light and introduced the short hand notation $b_c$ for the product of all constants in the total elastic cross-section times $2\pi N$. If we now neglect the very weak (logarithmic) energy dependence of $S\beta^2$, Eq. (40) becomes

$$
G_l \approx \frac{b_c \,\Delta E}{\tilde{\beta}^2 S(\tilde{E})} \frac{1}{\Delta E} \int\limits_{E_f}^{E_i} \mathrm{d}E \, Q_l(E).
\tag{41}
$$

---

[5] Any energy-loss mechanism may be used so long as its first two derivatives exist. However, we are anticipating use of the multiple-scattering distributions in a Class II condensed history scheme where events below some threshold are considered to be grouped and those above the threshold are treated discretely.

Here, $\Delta E = E_i - E_f$ is the energy loss during the step under consideration, $\tilde{E} = (E_i + E_f)/2$ the average energy of the electron and $\tilde{\beta}$ the velocity calculated from $\tilde{E}$. To carry out the $E$-integration we can perform a power series expansion in $\Delta E$,

$$
\int\limits_{E_f}^{E_i} \mathrm{d}E \, Q_l(E) \approx \Delta E \, Q_l(\tilde{E})\left[1 + \frac{\Delta E^2}{24} \frac{Q_l''(\tilde{E})}{Q_l(\tilde{E})} \pm \cdots\right],
\tag{42}
$$

where $Q_l''$ is the second derivative of $Q_l$ with respect to $E$. Using Eq. (18) for $Q_l$ and neglecting terms of the order of $\eta$ and terms small compared to $\ln(1/\eta)$, we arrive at the result

$$
\begin{aligned}
G_l &\approx \lambda_{\mathrm{eff}} Q_l(\tilde{E}), \\
\lambda_{\mathrm{eff}} &= \frac{b_c \Delta E}{\tilde{\beta}^2 S(\tilde{E})} \left[1 + \frac{4 + 6\tilde{\tau} + 3\tilde{\tau}^2}{3(2+\tilde{\tau})^2} \frac{\epsilon^2}{(2-\epsilon)^2}\right],
\end{aligned}
\tag{43}
$$

where $\tilde{\tau}$ is the ratio of the average electron kinetic energy to its rest mass energy and $\epsilon = \Delta E/E_i$ the energy-loss fraction. That means, when energy loss is taken into account, the multiple-scattering distribution is to a good approximation equivalent to the multiple-scattering distribution without energy loss resulting from $\lambda_{\mathrm{eff}}$ elastic collisions of electrons with the energy $\tilde{E}$. With this observation we can easily apply the theory developed in the previous sections to realistic calculations with electron energy loss taken into account.

To test the accuracy of the approximations leading to Eq. (43), we have calculated the multiple-scattering distribution resulting from the exact GS-moments $G_l$ and compared it to the distribution obtained with the approximated $G_l$'s given in Eq. (43) for various energies, materials and energy-loss fractions. The energy integration in Eq. (40) was done by a 32-point Gauss–Legendre quadrature. The disagreement between the exact and approximated distributions increases with increasing $\epsilon$. The maximum deviation found for $\epsilon = 25\%$ was of the order of 1%. For $\epsilon \leqslant 10\%$ the agreement was almost perfect. The ratio of the approximated to the exact distribution for $\epsilon = 10$, 25 and 33% is shown for typical cases in Fig. 4.

### Multiple–scattering ratios
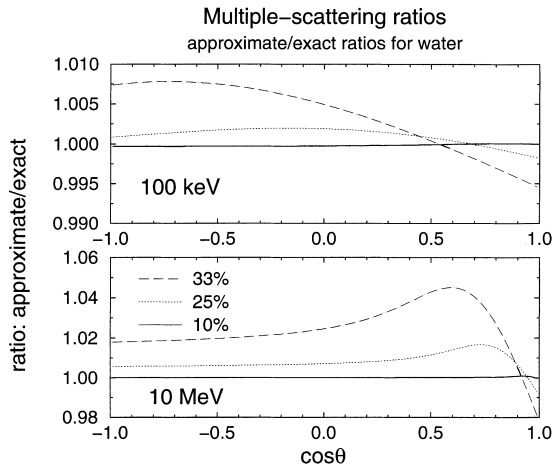approximate/exact ratios for water



Fig. 4. Ratio of the exact-MS distribution to the MS-distribution with energy loss taken into account according to Eq. (43) for 100 keV and 10 MeV electrons in water and energy-loss fractions $\epsilon$ of 10, 25 and 33%. For other energies and materials, similar dependence on the energy-loss fraction $\epsilon$ is observed.

## 5. Conclusions

A compact numerical representation of the Goudsmit–Saunderson multiple-scattering distribution has been calculated using the screened Rutherford elastic cross section with a Molière screening factor. The 360 kB of data represents the scattering distribution over a range of distance $1 \leqslant \lambda \leqslant 10^5$ measured in terms of elastic collision mean-free-paths, screening parameters covering a wide dynamic range and all scattering angles. The scaling function essentially removes all of the "forward-directedness" of the distribution leaving a surface that is optimally flat and suitable for rapid interpolation in Class II condensed-history schemes. The interpolation accuracy is 0.2% or better. For adaptation into Class II algorithms where the subthreshold interactions are treated in the CSDA, we have developed a method that allows for energy losses of up to 25% with a filling accuracy of about 1%. These developments should allow high-accuracy Monte Carlo transport in the approximation that the screened Rutherford elastic cross section with a Molière screening factor is adequate to describe the elastic physics. If it is not, it is possible that the technique developed herein could be extended to more accurate cross sections.

## References

[1] M.J. Berger, Monte Carlo calculation of the penetration and diffusion of fast charged particles, in: B. Alder, S. Fernbach, M. Rotenberg (Eds.), Methods in Comput. Phys., vol. 1, Academic Press, New York, 1963, pp. 135–215.

[2] S.A. Goudsmit, J.L. Saunderson, Phys. Rev. 57 (1940) 24–29.

[3] S.A. Goudsmit, J.L. Saunderson, Phys. Rev. 58 (1940) 36–42.

[4] D.W.O. Rogers, A.F. Bielajew, Monte Carlo techniques of electron and photon transport for radiation dosimetry, in: K. Kase, B. Bjärngard, F. Attix (Eds.), The Dosimetry of Ionizing Radiation, vol. III, Academic Press, New York, 1990, pp. 427–539.

[5] G.Z. Molière, Z. Naturf. 3a (1948) 78–97.

[6] A.F. Bielajew, Nucl. Instr. and Meth. B 86 (1994) 257–269.

[7] H.A. Bethe, Phys. Rev. 89 (1953) 1256–1266.

[8] P. Andreo, J. Medin, A.F. Bielajew, Med. Phys. 20 (1993) 1315–1325.

[9] A.F. Bielajew, Nucl. Inst. and Meth. B 111 (1996) 195–208.

[10] M.J. Berger, R. Wang, Multiple-scattering angular deflections and energy-loss straggling, in: T. Jenkins, W. Nelson, A. Rindi, A. Nahum, D. Rogers (Eds.), Monte Carlo Transport of Electrons and Photons, Plenum Press, New York, 1989, pp. 21–56.

[11] G.Z. Molière, Z. Naturf. 2a (1947) 133–145.

[12] N.F. Mott, Proc. Roy. Soc. London A 124 (1929) 425.

[13] N.F. Mott, Proc. Roy. Soc. London A 135 (1932) 429.

[14] S.T. Perkins, D.E. Cullen, S.M. Seltzer, Tables and Graphs of Electron-interaction Cross Sections from 10 eV to 100 GeV Derived from the LLNL Evaluated Electron Data Library (EEDL), Z = 1–100, Lawrence Livermore National Laboratory Report UCRL-50400, vol. 31, Livermore, CA (1991).

[15] W. Bothe, Z. Phys. 5 (1921) 63–69.

[16] G. Wentzel, Ann. Phys. 69 (1922) 335–368.

[17] K.B. Winterbon, Nucl. Instr. and Meth. B 21 (1987) 1–7.

[18] I. Kawrakow, Nucl. Instr. and Meth. B 108 (1996) 23–34.

[19] M. Abramowitz, I.A. Stegun (Eds.), Handbook of Mathematical Functions with Formulae, Graphs and Mathematical Tables, Number 55 in Applied Mathematics, National Bureau of Standards, Washington, DC, 1964.

[20] H.W. Lewis, Phys. Rev. 78 (1950) 526–529.

[21] A.F. Bielajew, D.W.O. Rogers, PRESTA: The parameter reduced electron-step transport algorithm for electron Monte Carlo transport, National Research Council of Canada Report PIRS-0042 (1986).

[22] A.F. Bielajew, D.W.O. Rogers, Nucl. Instr. and Meth. B 18 (1987) 165–181.

[23] S.M. Seltzer, Internat. J. Appl. Radiation and Isotopes 42 (1991) 917–941.

[24] L.V. Spencer, Phys. Rev. 98 (1955) 1597–1615.

[25] S. Wolfram, Mathematica: A System for Doing Mathematics by Computer, Addison–Wesley, Redwood City, CA, 1991.